Journal of Power Sources 241 (2013) 320–329

Contents lists available at SciVerse ScienceDirect

Journal of Power Sources

journal homepage: www.elsevier.com/locate/jpowsour

A neural network estimator of Solid Oxide Fuel Cell performance for on-field diagnostics and prognostics applications

Dario Marra [a], Marco Sorrentino [a], Cesare Pianese [a,*], Boris Iwanschitz [b]

[a] Department of Industrial Engineering, University of Salerno, Via Giovanni Paolo II 132, 84084 Fisciano (SA), Italy
[b] HEXIS AG, Zum Park 5 Postfach 3068, 8404 Winterthur, Switzerland

HIGHLIGHTS

- Nonlinear modelling of Solid Oxide Fuel Cell.
- Neural Network model for Solid Oxide Fuel Cell performance.
- Solid Oxide Fuel Cell model for diagnostic and prognostic applications.
- On-field monitoring of Solid Oxide Fuel Cell degradation.

ARTICLE INFO

Article history:
Received 3 February 2013
Received in revised form
9 April 2013
Accepted 23 April 2013
Available online 30 April 2013

Keywords:
Solid Oxide Fuel Cell
Neural network
Diagnosis
Degradation
Nonlinear modelling

ABSTRACT

The paper focuses on the experimental identification and validation of a neural network (NN) model of solid oxide fuel cells (SOFC) aimed at implementing on-field diagnosis of SOFC-based distributed power generators. The use of a black-box model is justified by the complexity and the incomplete knowledge of SOFC electrochemical processes, which may be awkward to simulate given the limited computational resources available on-board in SOFC systems deployed on-field. Suited training procedures and model input selection are proposed to improve NNs accuracy and generalization in predicting voltage variation due to degradation. Particularly, standing the interest in condition monitoring of SOFC performance throughout stack lifetime, input variables were selected in such a way as to account for the time evolution of SOFC stack performance. Different SOFC stacks outputs were tested to assess the generalization capabilities when extending NN prediction to those stacks for which no training data were gathered. The simulations performed on the test sets show the NN ability in simulating real voltage trajectory with satisfactory accuracy, thus confirming the high potential of the proposed model for real-time use on SOFC systems.

0. Introduction

In the last years solid oxide fuel cells have been gaining increasing attention, mainly for their potential use as stationary power generators as well as auxiliary power units (APUs) for transportation use (ground, marine, air). SOFC attractiveness lies on both the high energy conversion efficiency and the zero toxic emission levels (only the CO_2 released by the hydrogen production process is a concern). Other advantages include: modularity, fuel flexibility and low noise. Moreover, the high working temperatures provide additional positive features, such as potential use of SOFC in highly efficient cogeneration applications. SOFC are also suitable for internally reforming the fuel (e.g. natural gas, propane, methanol, gasoline, Diesel, etc.), thus avoiding the adoption of highly sophisticated and expensive external reformer, simplifying fuel storage as well. The big challenges to promote SOFC systems diffusion into the market are mainly related to production costs and durability. The achievement of these targets will surely contribute to enhance the technology deployment and finally starting a mass production phase. Besides costs and performance, long-term stability is an important requirement for the commercial application of the SOFC technology. For stationary applications, the commercial lifetime requirement is generally more than 40,000 h. However, these lifetime requirements have not been met yet: SOFC system prototypes still suffer from a low reliability of both the fuel cell itself and the complete system [1,2]. The state of the art of cell degradation mechanisms has not provided yet solid theories to support a reliable forecasting of SOFC stacks lifetime; among others SOFC operating conditions may cause a wide variety of ageing processes (e.g. high fuel utilization, carbon deposition, oxidation of the interconnect due to high temperature conditions) as well as mechanical stresses leading to, e.g. leakage or contact losses in

* Corresponding author. Tel.: +39 089964081; fax: +39 089964037.
E-mail address: pianese@unisa.it (C. Pianese).

0378-7753/$ – see front matter © 2013 Elsevier B.V. All rights reserved.
http://dx.doi.org/10.1016/j.jpowsour.2013.04.114

electrodes, these degradation processes considerably weighing upon lifetime [3,4]. Several theories and models are available in the literature [1,2,5] but none of them is able to provide effective lifetime predictions.

The paper focuses on the experimental identification and validation of a neural network (NN) estimator of SOFC output voltage aimed at enhancing on-field diagnosis and control of SOFC-based distributed power generators. Apart from the lack of both SOFC degradation mechanisms knowledge and models, the use of a black-box model is also justified by its low computational time, which makes it suitable for on-line uses. So far, most of existing models are based on physical conversion laws and governing equations [6–9]. Although being useful for design analysis and optimisation of SOFC, they are too complex for control and diagnosis of SOC system. This drawback impelled some researchers [10–17] to attempt black-box methods. The black-box are input–output (i.e. mapping) models, derived through statistical data-driven approach. Contrary to physical models, they are not based on explicit physical equations but use large databases with experimental data, which represent the behaviour of the modelled system as function of different operating, control and state variables.

Black-box models are built without exploiting any physical law, only a set of input–output pairs for training procedure is used instead. It has been demonstrated that the black-box models based on artificial intelligent approaches are very suitable for non-linear systems [18]. However, such models require a large amount of experimental data (i.e. training examples), which should well represent the behaviour of the system; therefore, the experimental burden for collecting meaningful data might become excessive. Although the experimental load may be considered as the main drawback of artificial intelligence-based modelling techniques, their intrinsic high accuracy represents the most attractive characteristic. These two opposite features lead to the main trade-off to deal with when approaching the modelling problem to be solved.

Arriagada et al. [10] proposed a non-linear fuel cell model by using neural networks (NNs) for evaluating SOFC performance; their model is a two-layer feed-forward network whose outputs are air flow, current density, temperatures of outlet air and fuel, average solid and reversible voltage. The model was trained via Backpropagation algorithm with a reduced amount of input and correct output data pairs generated by a physical cell model. Comparing the outputs of the NN model with that of the physical model, the average values of the errors are well below 1% and the maximum below 4%.

Milewski et al. [17] used the same NN structure of [10] to simulate the SOFC behaviour, using experimental data for training and testing process. Their SOFC model predicts the output cell voltage making use of 9 input parameters (current density, cathode inlet O_2 and N_2 flow densities, anode H_2 and He flow density, anode thickness, anode porosity, electrolyte thickness and electrolyte temperature). The testing results show that the NN can be successfully used in modelling the single solid oxide fuel cell.

Main contribution of this work, with respect to the above-mentioned works of [10,17], relates to the use of training and test sets suitable to include time among input variables, thus providing the developed NN with extended prediction capability, particularly those concerning degradation effects.

In this paper the first section is dedicated to the description of the working principles of SOFC systems, of the system analysed and of the selection of model input variables. The second section is focused on the description of neural networks and particularly on the parameter identification procedure used herein. In the third section the choice of the training and test sets is discussed. Finally the results are presented and commented via comparison of model outputs and experimental data.

1. SOFC working principle and black-box model input selection

Fuel cells are electrochemical devices capable of converting the chemical energy held by a hydrogen-rich fuel into electricity. Such conversion is direct, in that no intermediate combustion occurs [19]. Fuel cell working principle was discovered by Friedrich Schönbein, who found the fuel cell principle in 1838. Based on Schönbein publication Grove started his research and built the first fuel cell in 1839 [20]. A single cell consists of three main components: an anode, a cathode and a solid electrolyte separating the two electrodes. Oxygen and hydrogen (i.e. the reactants) are supplied to cathode and anode, respectively (see Fig. 1). Under electrical load, at the cathode surface the presence of perovskite catalyst enables oxygen ionization. The solid electrolyte allows the flux of oxygen ions to the anode, where they electro-oxidize hydrogen, thus releasing heat, water and electrons. Since electrolyte material ensures quasi-zero electronic conductivity, electrons are forced to flow through interconnect and external load towards the cathode, thus closing the electrical loop. In a SOFC the oxygen ions are formed at the cathode where the oxygen of the supplied air is reduced, whereas at anode hydrogen rich gas is oxidized releasing electrons and water, as sketched in Fig. 2. At the anode hydrogen rich gas must be supplied; almost any gas composition is tolerated by the anode materials except sulphur compounds. This feature allows the use of any reformate gas from either methane or liquid fuels, therefore the gas composition may affect the performance of the cell. Another distinctive characteristic of SOFC is the high operating temperature (usually $> 700\ ^\circ C$), which represents a relevant feature allowing the use of these systems for cogeneration of heat for practical applications. On the other hand, the high temperatures involved do not allow tight transient operations, which may entail changes in the thermal regime, which in turn may cause mechanical stresses in the materials.

To obtain the target electrical power, several cells are assembled together to form a stack, whose voltage and current outputs depend on the proper combination of parallel and series electrical connections among the cells. Moreover, to guarantee the proper operations of the stack some devices (i.e. balance of plant–BoP) are required to provide the right amount of reacting gases (i.e. air and reformate/hydrogen) as well as to manage the outflow hot gases for heat recovery. Besides the prereformer, which provides the reformate gas to the anode, the standard equipments of the BoP are: a blower for cathodic air supply; a set of heat exchangers, for inlet gases heating and outlet gases heat recovery; a post burner, to convert the residual anodic gas chemical energy into heat; a set of valves, for the fluid and thermal managements guaranteeing both performance optimization and thermal stresses control of the stack

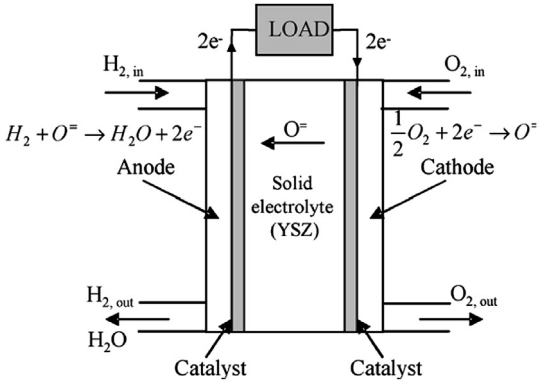

Fig. 1. SOFC basic principle.

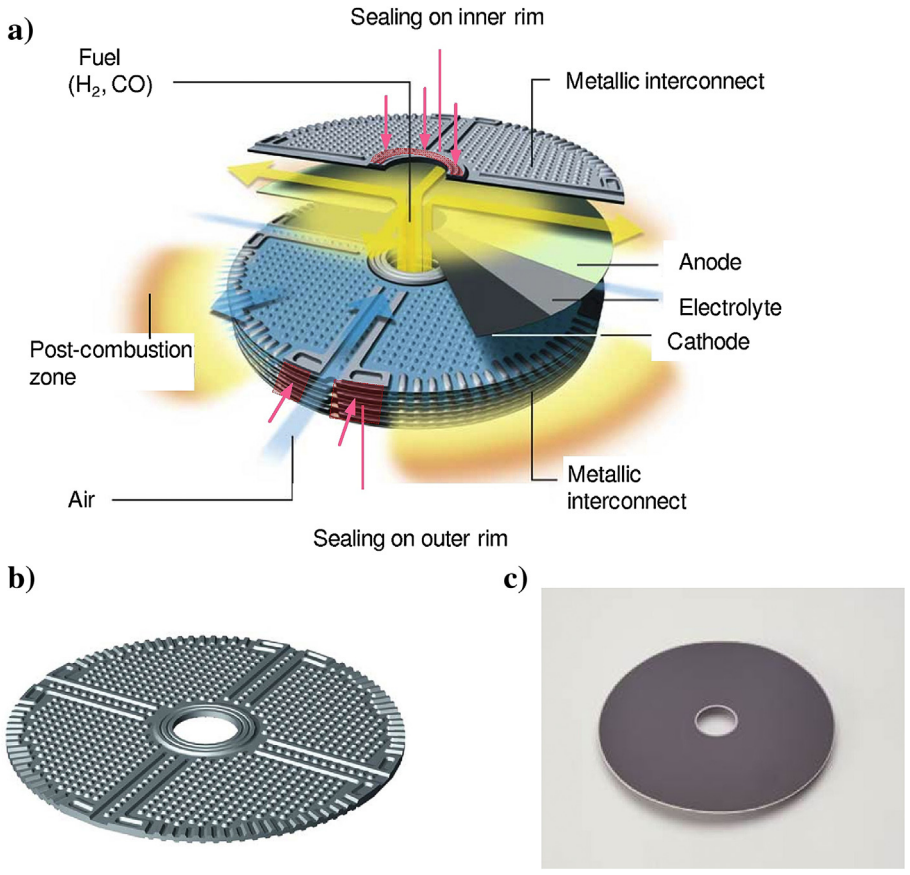

Fig. 2. a) Stack sketch; b) Metallic interconnect (MIC); c) Electrolyte supported cell (ESC).

materials. The complex interaction among BoP and stack requires well-designed control strategies to optimize system (Stack and BoP) performance as well as advanced diagnosis algorithms for fault management to avoid failures, which in turn may improve lifetime [3,4,21]. Therefore, an accurate stack voltage model is mandatory for model-based control, monitoring and diagnosis schemes as well as for prognostic algorithms implementation.

The SOFC stack modelled in this work is a 5-cells test rig produced by HEXIS AG (CH). In Table 1 the main specifications are reported [22]. This stack can be operated in the range [850–900]°C and consists of 100 cm^2 cells containing disk-shaped electrolyte supported cells (ESC) and metallic interconnects (MICs), see Fig. 2; these components are of planar design, with a round hole in the centre. Natural gas from the grid is converted by a catalytic partial oxidation (CPO) and supplied to the cells via the centre, while preheated air flows from the outside through 4 opposite radial channels onto the metallic interconnect, therefore both cathodic and anodic gases have parallel radial flows moving towards the stack periphery. The stack may be classified as a radial-planar co-flow. The post combustion takes place in the surrounding area of the stack [22].

Table 1
Main specifications of the 5-cells test rig.

Fuel cell	
Output	About 95 W
Type	Solid oxide fuel cell (SOFC)
Fuel	Natural gas
Fuel processing	Catalytic partial oxidation (CPO)
Configuration	Radial co-flow

1.1. Neural network input selection

For the definition of the input variables of a black-box model, the knowledge of the main phenomena occurring into the system being modelled is required; from a methodological point of view the authors have exploited the experience gained in other researches devoted to the black-box modeling of energy systems [23]. In the current study, the stack voltage is the output of the model and it has to be mapped with respect to the input variables of the model. Before describing the physical relationship among stack voltage and operating, control and state variables, it is worth noting that an accurate selection of these variables has to be performed to avoid data redundancy, which in turn may determine an increase of model's parameters leading to a loss of generality of the model [23]. At the same time the inputs selection must provide all the information necessary for the simulation of the output. For an effective selection of the input variables, the main electrochemical processes were analysed through the study of the voltage models [24,25] as reported below.

The ideal potential difference between anode and cathode is described via the Nernst equation:

$$E_{\text{Nernst}} = -\frac{\Delta G_{ox}(T_s)}{n_e F} - \frac{RT_s}{n_e F}\ln\left(\frac{p_{H_2O}}{p_{H_2}\sqrt{p_{O_2}}}\right) \quad (1)$$

The Nernst potential is reduced due to the three major polarization losses: activation, Ohmic and concentration, thus the voltage can be written as:

$$V_s = E_{Nernst} - V_{Act} - V_{Ohm} - V_{Conc} \quad (2)$$

1.1.1. Activation losses

Activation losses represent the energy barrier to be overcome to activate the electrochemical reactions occurring at the electrodes surface. This amount of energy inevitably causes a significant voltage loss, which is usually modelled through the non-linear relationship known as Butler–Volmer equation [26]:

$$V_{Act} = \frac{RT_s}{\alpha(T_s)F}\sinh^{-1}\left(\frac{j}{2j_0(T_s)}\right) \tag{3}$$

where α is the charge transfer coefficient and j_0 is the exchange current density.

1.1.2. Ohmic losses

Ohmic losses mainly depend on the electronic conductivity of electrodes and the ionic conductivity of the electrolyte. Such losses are estimated summing up the contribution from each cell component (i.e. anode, cathode and electrolyte), as follows:

$$\begin{aligned} V_{Ohm,k} &= \frac{l_k}{\sigma_k(T_s)}\cdot j \\ V_{Ohm} &= \sum_k V_{Ohm,k} \qquad k = [an, ca, el] \end{aligned} \tag{4}$$

1.1.3. Concentration losses

As fuel is consumed, hydrogen and oxygen partial pressures decrease at anode and cathode, respectively. The depletion rate depends on average current density drawn from the cell. As the current density increases, the partial pressures decrease and eventually an insufficient amount of reactants are available at the electrodes. This results in significant losses until the voltage is reduced to 0 [20,27]. When fuel or/and oxygen starvation occurs the current approaches high current densities towards its limiting value. The concentration losses are estimated as follows:

$$V_{Conc} = -\frac{RT_s}{2F}\left[\frac{1}{2}\ln\left(1-\frac{j}{j_{cs}}\right)+\ln\left(1-\frac{j}{j_{as}}\right)-\ln\left(1+\frac{p_{H_2}j}{p_{H_2O}j_{as}}\right)\right] \tag{5}$$

The anode and cathode limiting currents (i.e. j_{as} and j_{cs}, respectively) can be computed as function of species diffusion coefficients, as proposed by Ref. [24].

The electrochemical models highlight the functional dependence of the stack voltage to some physical quantities. In a fuel cell these variables change along the flows directions and their spatial distributions are governed by energy, mass and momentum balances occurring inside the cell. With reference to the steady-state model proposed by [25], the SOFC stack voltage was expressed as a function of the following variables:

$$V_s = f\left(\begin{matrix}\bar{j}, T_{air,ca,in}, T_{fuel,an,in}, T_{s,in}, x_{H_2,an,in}, x_{CO_2,an,in}, x_{CO,an,in}, x_{CH_4,an,in}, \\ x_{H_2O,an,in}, x_{O_2,ca,in}, \dot{m}_{fuel,an,in}, \dot{m}_{air,ca,in}\end{matrix}\right) \tag{6}$$

The input species at the anode inlet were supposed to be in chemical equilibrium and their concentrations ($x_{i,an,in}$) were supposed to be related to the temperature ($T_{fuel,an,in}$) of the gas blend coming from the CPO pre-reformer and entering the anode. According to this hypothesis eq. (6) can be simplified as follows:

$$V_s = f\left(\bar{j}, T_{air,ca,in}, T_{fuel,an,in}, T_{s,in}, \dot{m}_{fuel,an,in}, \dot{m}_{air,ca,in}\right) \tag{7}$$

According to the hypothesis assumed for the model proposed in literature [25], for a co-flow configuration the temperature of the stack was supposed to be equal to that of the anode and cathode gas streams. Thus only the fuel inlet temperature was considered and the stack voltage was expressed by eq. (8):

$$V_s = f\left(\bar{j}, T_{air,ca,in}, \dot{m}_{fuel,an,in}, \dot{m}_{air,ca,in}\right) \tag{8}$$

The stack was fuelled by methane and a CPO was present in the system, the fuel mass flow considered as input to the model was the methane mass flow at the CPO inlet.

The choice of the methane flow rate at CPO inlet and not directly to the anode was linked to the difficulty to measure in the real system analysed, the methane flow rate directly at the anode inlet. The methane (and hydrogen) flow rates at the anode inlet are linked to the CPO conversion efficiency. The two main factors that affect CH_4 to H_2 conversion of the CPO efficiency are the catalyst bed temperature and the ratio of the reactants (CH_4 and O_2) [28,29]. At proper CPO operating temperature, the amount of hydrogen created depends on the supply rate of CH_4 and the CPO air to fuel ratio, more specifically, the oxygen to carbon ratio. The oxygen to carbon ratio also influences the amount of heat generated in the CPO, which then affects the CPO catalyst bed temperature, thus also the temperature of the gas blend coming from the pre-reformer and entering the anode ($T_{fuel,an,in}$). In the present work the conversion efficiency of the CPO and thus the methane and hydrogen flow rates at anode inlet were assumed to be function of the methane flow rate at CPO inlet and of the gas blend temperature of CPO outlet.

$$\dot{m}_{fuel,an,in} = f_2\left(\dot{m}_{CH_4,CPO,in}, T_{fuel,an,in}\right)$$

According to the hypothesis assumed the stack voltage can be expressed:

$$V_s = f\left(\bar{j}, T_{air,ca,in}, \dot{m}_{CH_4,CPO,in}, \dot{m}_{air,ca,in}\right) \tag{9}$$

As already mentioned above, the SOFC stacks are characterized by complex degradation phenomena during their life causing a reduction of the stack voltage. The stack degradation is usually divided into two main classes: the steady state degradation due to the ageing of stack components, which cannot be avoided, and the degradation accelerated or caused by transient operating conditions e.g. redox- and thermo-cycling or BoP failures [5]. Degradation processes are still not completely understood and thus cannot be explicitly modelled with a black-box mapping model, unless large dedicated experiments are available, but model generality may not be guaranteed. To account for the voltage time evolution induced by degradation, the time is considered as further input of the NN model. Finally the stack voltage was expressed as a function of: anode inlet temperature, stack average current density, CPO inlet fuel methane mass flow, air mass flow at cathode inlet and time, as represented in eq. (10):

$$V_s = f\left(\bar{j}, T_{air,ca,in}, \dot{m}_{CH_4,CPO,in}, \dot{m}_{air,ca,in}, t\right) \tag{10}$$

A sketch of the input–output structure of the model is shown in Fig. 4, where also the links among input, intermediate and output

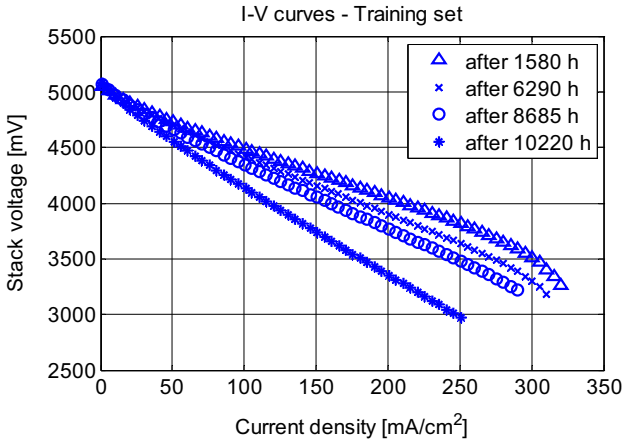

Fig. 3. Stack voltage vs current density at different operating hours (Training set, *I–V* curves).

computing elements (i.e. neurons) are reported. Therefore, the time is considered as an index of the degradation. The degradation causes an increase in cell polarization losses, whose effect is the rotation of the current–voltage (*I–V*) curves in time, as shown in Fig. 3. It is important noting that the effect of natural degradation (ageing) is present both in the *I–V* curves and in long-term sets. It is finally worth noting that operating temperature was not included as input in eq. (10) since the experimental curves showed later on in the paper were acquired for a furnace temperature set to 900 °C.

2. Neural networks

In this work, multi-layer-perceptron-feed-forward (MLPFF [30]) neural networks were adopted to develop accurate models for predicting Hexis SOFC stack voltage, as shown on Fig. 4. MLPFF parameters identification is performed through a learning process during which a set of training examples (experimental data) is presented to the network to settle the levels of the connections between the nodes. The most common approach is the error Backpropagation algorithm, due to its easy-to-handle implementation. At each iteration the error between the experimental data and the corresponding estimated value is propagated backward from the output to the input layer through the hidden layers. The learning process is stopped when the following cost function (MSE) reaches its minimum:

$$MSE(\theta) = \frac{1}{N}\sum_{i=1}^{N}(\hat{y}_i - y_i)^2 \qquad (11)$$

where N is the size of the training pattern gathered from available experiments. The above function minimization can be carried out in either a batch or a pattern-by-pattern way. The former is usually preferred at the initial development stage, whereas the latter may be adopted online to enable network weights adaptation in response to the exogenous variations of the controlled/simulated

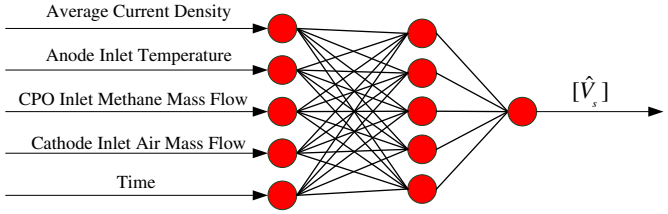

Fig. 4. Sketch of the input–output model; the structure of the neural networks is described into Section 2.

system. The Backpropagation method is a first-order technique and its use for complex networks might cause long training and in some cases a loss of effectiveness of the procedure. Therefore, in the current work a second-order method based on the Levenberg–Marquardt optimization algorithm is adopted [30–34].

The training process aims at determining NN models with a satisfactory compromise between precision (i.e. small error on the training-set) and generalization (i.e. small error on the test-set). High generalization can be guaranteed only if the training data-set is sufficiently rich, so as to cover most of the system operating domain, as shown on Fig. 5.

As far as network structure and learning approach are concerned, the precision and generalization goals are often in conflict. The loss of generalization due to parameters redundancy in model structure is addressed in the literature as overfitting [35]. This latter may occur in case of a too large number of weights, which in principle improves NN precision but may cause generalization to decrease. A similar effect can occur if network training is stopped after too many epochs. Although this can be beneficial to precision, it may negatively impact generalization capabilities and is known as overtraining. Based on the above considerations and to ensure a proper design of NNs, the following steps should be accomplished:

i) generate a training data set extensive enough to guarantee acceptable generalization of the knowledge retained in the training examples,
ii) select the proper stopping criterion to prevent overtraining, and
iii) define the network structure with the minimum number of weights.

As for the impact of point i) on the current application, the influence of the main input variables (i.e. load and SOFC degradation over time) was satisfactorily taken into account when selecting the most appropriate training set and network inputs, as deeply described in the following section. Point ii) is usually addressed by employing the early stopping method [33]. This technique consists of interrupting the training process, once the MSE computed on a data set different from the training one stops decreasing. Therefore, when the early stopping is used, network training and test require at least three data sets [31]: training-set (set A), early stopping test-set (set B) and generalization test-set (set C). In this work, the NN training subject to early stopping criterion was performed in Matlab® environment. Fig. 6 shows the evolution in time of the NN MSE on both set A and set B, highlighting how the learning process for the NN SOFC model here developed was as long as 53 epochs.

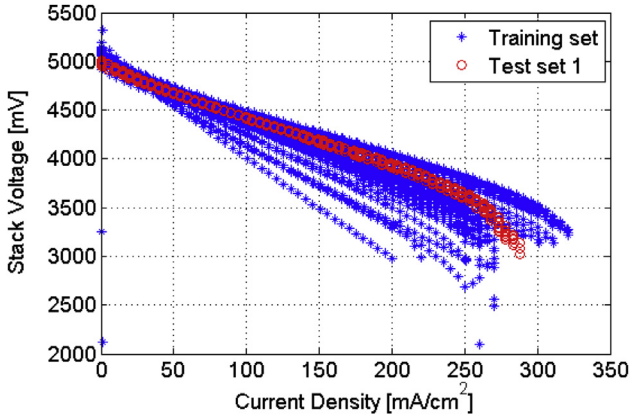

Fig. 5. Current Density-Stack Voltage domains covered by training-and test-sets. In order to ensure satisfactory NN generalization, the domain used as training-set is as wide as possible, and it fully includes the test-set.

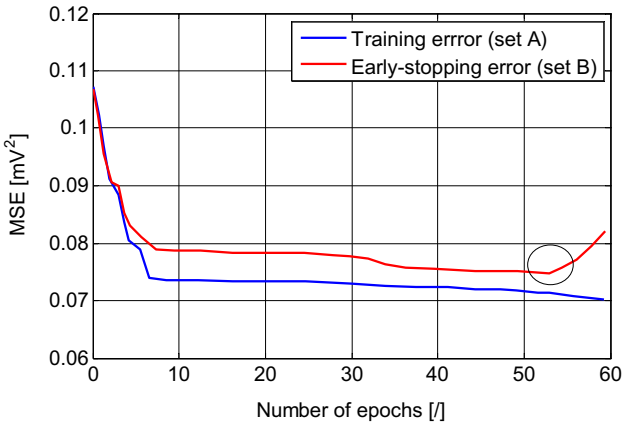

Fig. 6. NN MSE of training-set and early stopping test-set vs number of epochs.

Such an interruption occurred because the estimation error on set B (i.e. early stopping data set) stopped decreasing, as shown on Fig. 6, thus clearly indicating that the overtraining problem would have occurred if further training epochs had been performed.

Point iii) has been addressed, once the basic input variables (i.e. 5 input neurons) have been selected, by determining the network structure with optimal number of hidden layers and neurons. As for the former variable, the "universal approximation theorem" (theorem of existence of neural networks applied to Kolmogorov Cybenco, 1988 and Hornik, 1989) demonstrates that a 1 hidden layer NN ensures achieving satisfactory approximation accuracy for all continuous functions. Once the number of hidden layer is fixed to one, the number of hidden neurons must be defined. In order to prevent the NN training from the above-discussed overfitting issue, in the current work the optimal trade-off between network accuracy and dimension has been accomplished through a parametric analysis by varying the number of hidden neurons from 3 to 10. That study has been performed after the selection of the training set, whose details are given in the following section, leading to the definition of a neural network with 5 neurons in the hidden layer. According to the NN structure shown in Fig. 4 the neural network has 5 inputs, 5 hidden neurons ad 1 output; therefore the parameters of the model are 36, of which 30 weights, connecting the neurons and 6 biases, 1 per each neuron in the hidden layer and 1 on the output neuron.

In the following section the strategy adopted to ensure proper selection of training and test sets, is presented and discussed in detail.

3. Training and test data sets definition

As anticipated above and according to the system identification theory [36], two sets of data should be used for the NN training and for the generalization test, respectively. To guarantee the highest generalization the two sets should be independent and their selection must be performed carefully. Same principle applies to the early stopping data set, which may be a sub-set of either the training or the test sets. Owing to the low extrapolation capabilities of the NN, it is essential that the training set spans the domain of each input variable to its largest extent. It is worth recalling that the input variables were selected following the guidelines drawn in Section 1 and, according to that analysis, the methane flow rate, the air flow rate, the temperature of the reformate fuel, the current density and the time were chosen as input variables for the neural network model. After the input variables selection, the training set must be generated in such a way to reflect the data independence

Table 2
Features of the experimental data-sets used for neural network training and validation.

	I–V data	Long-Term data	Technology
Training set	YES	YES	1
Test set 1	YES		1
Test set 2	YES		2
Test set 3		YES	1
Test set 4		YES	1

principle just drafted; it has to guarantee the highest generalization with the minimum amount of training data, to avoid accuracy losses due to, e.g. the occurrence of overfitting. The selection of the training set is therefore critical and a trade-off between high number of measures and high information content of the database has to be solved. Advanced methodologies, such as experimental design [37,38], can support the design of experimental campaigns; nevertheless, the generation of new data entails an analysis of costs and time needed to build the new data set, on the other hand the system might not be on operation and available data must be used. When databases are already populated, several methodologies ranging from easy-to implement random-based selection up to complex ones, such as active selection of informative data [39] or more general data mining techniques [40,41] might be implemented.

The purpose of this work is to develop a neural network to estimate the voltage of SOFC stacks, which accounts for the system degradation over time. For this reason the data required for the development of the model (i.e. training data) must contain data measured continuously over a time period of few thousand hours. The Training set (see Table 2) was recorded at Hexis premises and contains the measurements acquired over a long time interval (see Fig. 7). Such a data set consists of two data groups: in the first set (see red circles in Fig. 7) all the operating conditions are constant, except for some points belonging to *I–V* curves, built up by changing occasionally the stack load (current density); whereas in the second one several current–voltage (*I–V*) curves (blue stars) are available at different time intervals; for these latter data group the stack control variables vary according to the different values imposed to stack current, spanning the current range from zero to its maximum value. The availability of Long-Term and *I–V* data makes the training data very appealing since the experimental data holds simultaneously the knowledge about the degradation process (Long-Term data) and the behaviour of the stack at different current levels (*I–V* curves), respectively. As a matter of fact, the availability

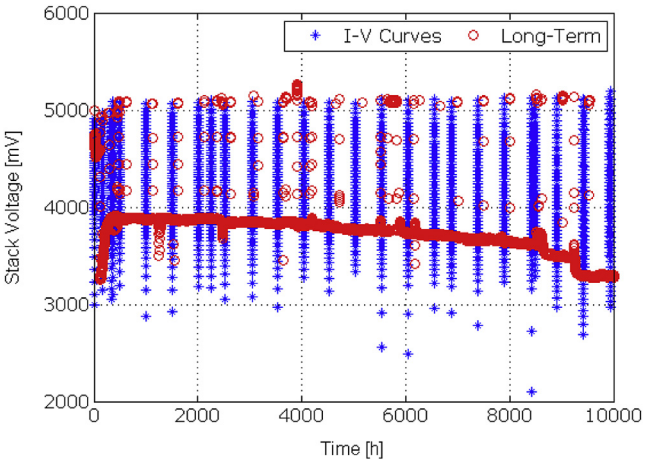

Fig. 7. *I–V* curves and long-term voltage data (Training set).

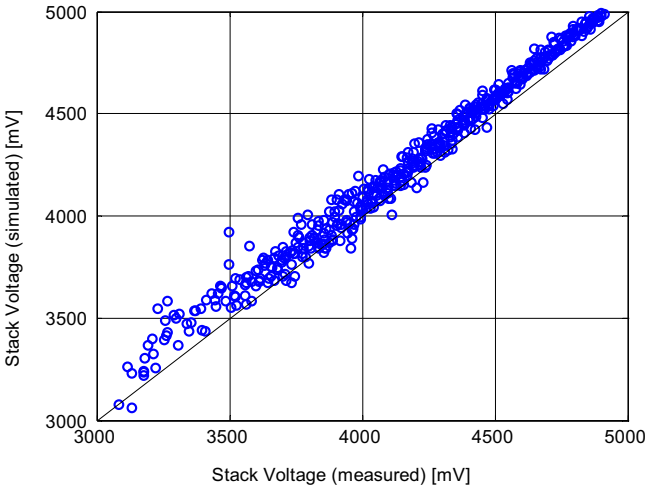

Fig. 8. Comparison between measured and simulated stack voltage on test set 1 (*I–V* curves).

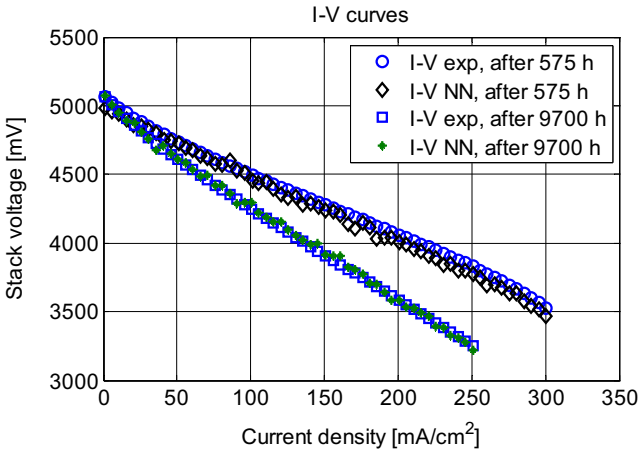

Fig. 10. Comparison between measured and simulated *I–V* curves for the training set.

of *I–V* curves recorded at different times also contributes to providing further knowledge content on degradation effect, as shown in Fig. 3, where the slope variation in the *I–V* relationship due to increasing degradation clearly emerges. Thanks to the non-linear capabilities of the neural network, the combined influence of degradation and input variables change can be simulated with high accuracy by the same model. Therefore, the model is suitable to monitor correct functioning of the stack even after expected degradation. Such capabilities are key features of model-based monitoring and diagnosis algorithms, especially to allow performing long-term prognosis for stack lifetime forecast.

To enlarge the training data-set, which in turn results in improved neural network generalization, data measured on two different stacks belonging to the same family (i.e. same material and geometry, Technology 1 in Table 2) were considered for parameters identification. The merging between the experiments acquired on the two stacks was possible since it was assessed that the discrepancies among voltage measured at the same operating conditions were safely negligible. The training set was constructed by joining the *I–V* curves and Long-Term data of the two stacks belonging to Technology 1. Care was given to cover the entire domain of the stack operating points; this was achieved by comparing the domains of the model inputs of the training set with those of the other data set (test sets). When building the training set, a balance between *I–V* curves and long-term test was pursued by selecting all the *I–V* curves and varying afterwards the number of long-term data to be included. Indeed it is mandatory to avoid that long series of data at constant operation polarize the behaviour of the model; moreover, the knowledge to be transferred to the network has to be balanced among the main processes considered for the training. The optimum ratio between *I–V* and long-term points was defined through a trial and error process, evaluating the generalization errors on different test sets. The choice of long-term data was done randomly by selecting single points from the entire data set. It is worth noting here that this procedure is valid for static neural network, whereas for dynamic neural network the time sequence has to be considered to simulate the dynamics of the system to be modelled [23,33]. Once the training data set was created, the sub-set for the early stopping was built by picking-up randomly the 12% of the data.

After the training, the generalization capabilities of the neural network were tested on four additional data-sets, whose data were not used during the training. These data were recorded at Hexis on two different stacks, one with the same technology considered for

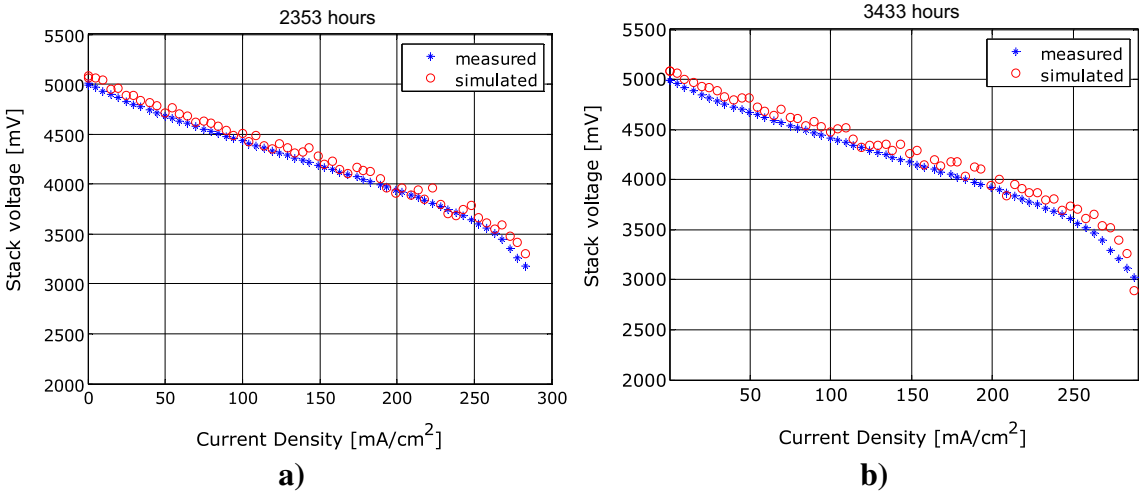

Fig. 9. a) Comparison between measured and simulated stack voltage for test set 1 (*I–V* curves) at 2353 h; b) Comparison between measured and simulated stack voltage for test set 1 (*I–V* curves) at 3433 h.

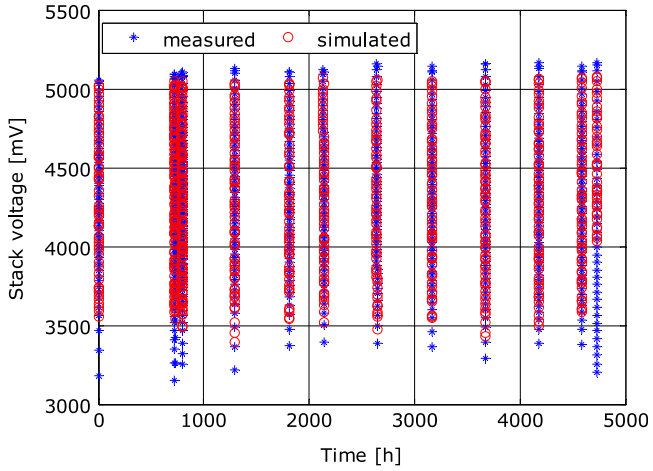

Fig. 11. Comparison between measured and simulated stack voltage for test set 2 (*I–V* curves).

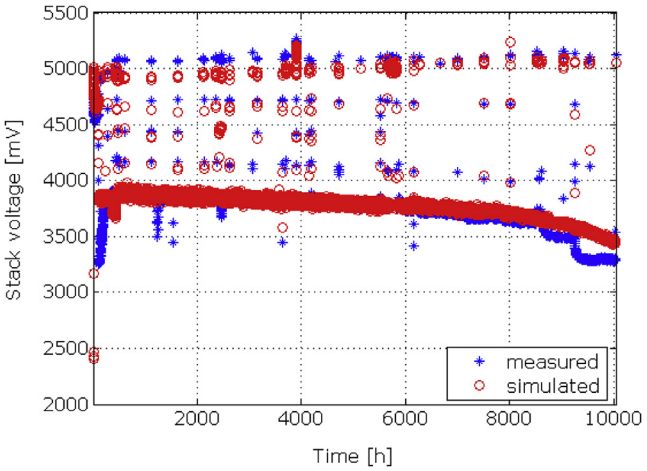

Fig. 13. Comparison between measured and simulated stack voltage for test set 3 (Long-Term).

the training (i.e. Technology 1 in Table 2) and another one with a different technology (i.e. different material and geometry, Technology 2 in Table 2). Therefore, the generalization capabilities of the model were properly checked by testing the ability of the neural network to reproduce the *I–V* curves and the voltage output of the Long-Term sets. Overall, the network was tested on the 4 test sets shown on Table 2, consisting of 2 *I–V* curves and 2 Long-Term sets.

4. Results

The neural network voltage simulator exhibited excellent accuracy for different *I–V* curves, as it is shown in the comparison between simulated and experimental (i.e. measured) data of Figs. 8 and 9, where the generalization capabilities of the trained network were verified on Test set 1 (see Table 2). The data set considered in Figs. 8 and 9 belongs to an SOFC stack of the same technology (i.e. Technology 1) as the one used for the training. In Figs. 9 and 10, it is possible to note how the neural network, thanks to the inclusion of time among the input variables, well simulates the change in *I–V* curve slopes, due to the "natural" stack degradation. Such a relevant feature of the developed neural network should be also attributed to the correct choice of the training set, which allowed a good coverage of the domain of model inputs, and the correct balance between the *I–V* curves and long-term data shares in the training set.

The following validation task consisted of further comparative analyses, conducted on *I–V* curves measured for a stack of a different technology from that used for training (i.e. Test set 2 in Table 2). Even in this case the network showed excellent results, as it can be seen in Figs. 11 and 12. This result can be explained considering that the new stack technology (i.e. 2) is comparable to the old one (i.e. technology 1 – the one used for training) from the performance point of view. Actually, the major change associated to technology 2 is in robustness (cycling stability and Long-Term degradation) and manufacturing. The performance and therefore the *I–V* characteristic are significantly close to each other. Indeed in the analysed current range (i.e. max 300 mA/cm^2) the main contribution to stack resistance comes from the gas conversion processes, which are highly dependent on the NN input parameters.

Also the accuracy attained by the neural network on long-term data was relevant, as shown in Figs. 13 and 14, which illustrate the comparison of experimental and simulated data on Test set 3 and Test set 4 (see Table 2), respectively. The network was able to simulate the entire trajectory of performance degradation, which as usual for fuel cells is expressed in terms of gradual reduction of stack voltage in time, while keeping the load constant. In Fig. 13, it is worth noting that the network, at the end of the experimental

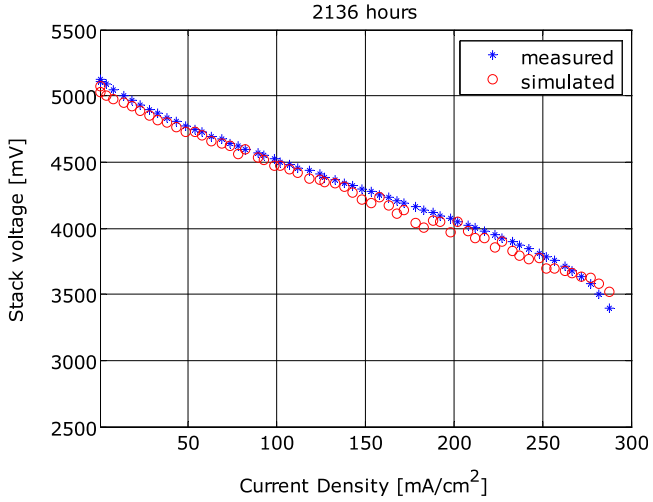

Fig. 12. Comparison between measured and simulated stack voltage for test set 2 (*I–V* curves) at 2136 h.

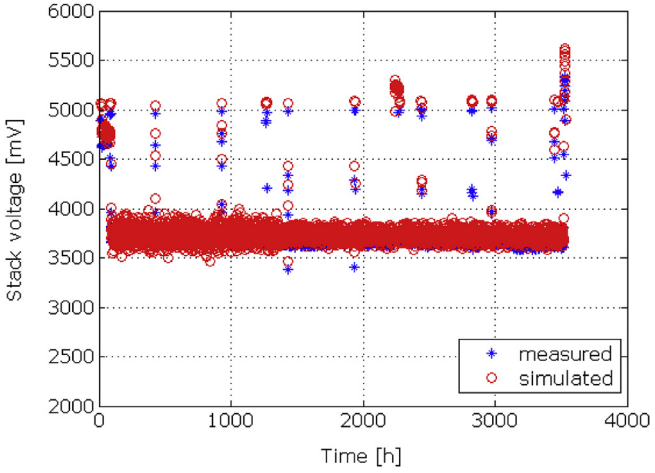

Fig. 14. Comparison between measured and simulated stack voltage for test set 4 (Long-Term).

trajectory, was only capable of simulating an average voltage reduction trend; such a behaviour can be explained considering that the developed network is intrinsically a static nonlinear model, thus not being able to precisely reproduce some dynamic manoeuvres. Nevertheless, the inclusion of time among the input variables still ensures obtaining good prediction of expected stack degradation in the next operating hours.

The results shown and discussed above are certainly a fair trade-off between the two different types of data, I–V curves and Long-Term data trajectories. It is important remarking here that the network could be trained with a more pronounced tendency towards one or the other type of data, depending on what is the targeted predictive information that has to be guaranteed in SOFC monitoring.

6. Conclusions

In this paper a neural network to simulate the voltage trajectory of an SOFC stack operated up to 10 thousand hours at constant load has been developed. The system analysed is a 5-cells test rig, produced by Hexis. The training set has been chosen appropriately, particularly aiming at finding the best trade-off between good knowledge of SOFC performance, expressed in terms of I–V curves, and degradation information, the latter being strictly linked to long-term data acquisition. The neural network exhibited excellent prediction accuracy, even for systems with different technology from the one used for training the model.

Beyond showing excellent prediction capabilities, the NN ensured high accuracy in well reproducing evolution of degradation in SOFC stacks, especially thanks to the inclusion of time among model inputs. The latter aspect is to be considered as a significant contribution of this paper, as it was proven effective to enable Multi Layer Perceptron Neural Networks, as the one proposed here, to well reproduce low frequency variations in SOFC behaviour, which are mainly induced by degradation effects. Therefore, the proposed neural network training procedure is a good candidate to address emerging needs in fuel cell development and on-field deployment, such as the opportunity of developing versatile model-based tools, which are required to be generic enough to be exploited for real-time control and diagnosis of different fuel cell systems typologies, technologies and power scales.

Acknowledgements

The results presented were obtained in the framework of a research cooperation between University of Salerno and Hexis AG. The research leading to these results has received funding from the University of Salerno (ex 60%) and from the European Union's Seventh Framework Programme (FP7/2007–2013) for the Fuel Cells and Hydrogen Joint Technology Initiative under grant agreement n° [245128] 10 (Project - GENIUS, GEneric diagNosis Instrument for SOFC systems).

Nomenclature

CPO	catalytic partial oxidation
E_{Nernst}	[V] Nernst ideal potential
F	[C mol^{-1}] Faraday constant
G	[J mol^{-1}] Gibbs free energy
j	[mA cm^{-2}] current density
$\bar{j}$	[mA cm^{-2}] average current density
j_0	[mA cm^{-2}] exchange current density
j_{as}	[mA cm^{-2}] anode limiting current density
j_{cs}	[mA cm^{-2}] cathode limiting current density
l	[cm] thickness
$\dot{m}_{air,ca,in}$	[g h^{-1}] cathode inlet air mass flow
$\dot{m}_{\text{CH}_4,\text{CPO},in}$	[g h^{-1}] CPO inlet CH_4 mass flow
$\dot{m}_{fuel,an,in}$	[g h^{-1}] anode inlet fuel mass flow
MSE	mean squared error
N	[/] Number of epochs
NN	neural network
n_e	[/] number of electrons
p_{H_2}	[Pa] hydrogen partial pressure
$p_{\text{H}_2\text{O}}$	[Pa] water partial pressure
p_{O_2}	[Pa] Oxygen partial pressure
R	[J mol^{-1} K] universal gas constant
SOFC	Solid Oxide Fuel Cell
t	[s] time
$T_{air,ca,in}$	[K] air temperature at cathode inlet
$T_{fuel,an,in}$	[K] fuel temperature at anode inlet
T_s	[K] Stack Temperature
$T_{s,in}$	[K] stack temperature at inlet section
V_{Act}	[V] activation losses
V_{Conc}	[V] concentration losses
V_{Ohm}	[V] Ohmic losses
V_s	[V] stack voltage
$x_{\text{CH}_4,an,in}$	[%] methane molar concentration at anode inlet
$x_{\text{CO},an,in}$	[%] monoxide molar concentration at anode inlet
$x_{\text{CO}_2,an,in}$	[%] dioxide molar concentration at anode inlet
$x_{\text{H}_2\text{O},an,in}$	[%] water molar concentration at anode inlet
$x_{\text{O}_2,an,in}$	[%] oxygen molar concentration at cathode inlet
y	experimental data
$\hat{y}$	network estimated output

Greek symbols

Δ	change
α	[/] charge transfer coefficients
θ	[/] neural network-parameters vector.
σ	[S cm^{-1}] ionic/electronic conductivity

Footers

air	air
an	anode
ca	cathode
el	electrolyte
fuel	fuel
in	inlet
ox	oxidation reaction
s	stack

References

[1] H. Yokokawa, H. Tu, B. Iwanschitz, A. Mai, Journal of Power Sources 182 (2008) 400–412.
[2] H. Tu, U. Stimming, Journal of Power Sources 127 (2004) 284–293.
[3] I. Arsie, A. Di Filippi, D. Marra, C. Pianese, M. Sorrentino, Fault tree analysis aimed to design and implement on-field fault detection and isolation schemes for SOFC systems, in: ASME 8th International Conference on Fuel Cell Science, Engineering and Technology, vol. 1, 2010, pp. 389–399.
[4] D. Marra, C. Pianese, M. Sorrentino, Implementation of a model-based methodology aimed at detecting degradation and faulty operation in SOFC systems, in: ASME 9th International Conference on Fuel Cell Science, Engineering and Technology, vol. 22, 2011, pp. 449–455.
[5] D. Larrain, J. Van herle, D. Favrat, Journal of Power Sources 161 (2006) 392–403.
[6] K. Wang, D. Hissel, M.C. Pera, N. Steiner, D. Marra, Sorrentino M. ., C. Pianese, M. Monteverde, P. Cardone, J. Saarinen, International Journal of Hydrogen Energy 36 (2011) 7212–7228.
[7] H. Yakabe, T. Ogiwara, M. Hishinuma, I. Yasuda, Journal of Power Sources 54 (2001) 102–144.
[8] K.P. Recknagle, R.E. Williford, L.A. Chick, D.R. Rector, M.A. Khaleel, Journal of Power Sources 14 (2003) 109–114. http://dx.doi.org/10.1016/S0378-7753(02)00487-1.
[9] X. Xue, J. Tang, N. Sammes, Y. Du, Journal of Power Sources 22 (2005) 142–211.

[10] J. Arriagada, P. Olausson, A. Selimovic, Journal of Power Sources 112 (2002) 54–60.
[11] U.K. Chakraborty, Energy 34 (2009) 740–751.
[12] E. Entchev, L. Yang, Journal of Power Sources 170 (2007) 122–129.
[13] D.E. Goldberg, Genetic Algorithms in Search, Optimization and Machine Learning, Addison-Wesley Educational Publishers Inc, 1989.
[14] H.B. Huo, X.J. Zhu, G.Y. Cao, Journal of Power Sources 162 (2006) 1220–1225.
[15] H.B. Huo, X.J. Zhu, W.Q. Hu, H.Y. Tu, J. Li, J. Yang, Journal of Power Sources 185 (2008) 338–344.
[16] J.S.R. Jang, Systems, Man and Cybernetics, IEEE Transactions 23 (1993) 665–685.
[17] J. Milewski, K. Swirski, International Journal of Hydrogen Energy 34 (2009) 5546–5553.
[18] K. Patan, Artificial Neural Networks for the Modelling and Fault Diagnosis of Technical Process, Lecture Notes in Control and Information Sciences, vol. 377, Springer, 2008, p. 206.
[19] K. Rajashekara, Propulsion System Strategies for Fuel Cell Vehicles, SAE Paper 2000-01-0369 (2000).
[20] J. Larminie, A. Dicks, Fuel Cell Systems Explained, John Wiley and Sons, Chichester, West Sussex (England), 2003, pp. 1–24, 207–227.
[21] M. Sorrentino, C. Pianese, Journal of Power Sources 196 (2011) 9036–9045.
[22] A. Mai, B. Iwanschitz, U. Weissen, R. Denzler, D. Haberstock, V. Nerlich, A. Schuler, ECS Transactions Solid Oxide Fuel Cells 12 35 (2011) 87–96.
[23] I. Arsie, C. Pianese, M. Sorrentino, Engineering Applications of Artificial Intelligence 19 (2006) 65–77.
[24] R. Braun, Optimal Design and Operation of Solid Oxide Fuel Cell Systems for Small-scale Stationary Applications, University of Wisconsin, Madison, USA, 2002. Doctoral dissertation.
[25] M. Sorrentino, C. Pianese, Y.G. Guezennec, Journal of Power Sources 180 (2008) 380–392.
[26] K. Keegan, M. Khaleel, L.A. Chick, K. Recknagle, S. Simner, J. Deibler, Analysis of a planar solid oxide fuel cell based automotive auxiliary power unit, SAE Technical Paper (2002). Series No. 2002-01-0413, pp. 1–12. http://dx.doi.org/10.4271/2002-01-0413.
[27] S.C. Singhal, K. Kendall, Solid Oxide Fuel Cells – Fundamentals, Design and Applications, Elsevier Ltd., Oxford, 2003, pp. 233–237.
[28] V. Recupero, L. Pino, R.D. Leonardo, M. Lagana, G. Maggio, Journal of Power Sources 71 (1998) 208–214.
[29] J. Zhu, D. Zhang, K.D. King, Fuel 80 (2001) 899–905.
[30] D.W. Patterson, Artificial Neural Networks – Theory and Applications, Prentice Hall, 1995.
[31] S. Haykin, Neural Networks, Prentice Hall, 1999.
[32] R. Hecht-Nielsen, Neurocomputing, Addison-Wesley, 1987.
[33] M. Nørgaard, O. Ravn, N.L. Poulsen, L.K. Hansen, Neural Networks for Modeling and Control of Dynamic Systems, Springer-Verlag, 2000.
[34] B.D. Ripley, Pattern Recognition and Neural Networks, Cambridge University Press, 2000.
[35] O. Nelles, Nonlinear System Identification: From Classical Approaches to Neural Networks and Fuzzy Models, first ed., Springer, Berlin, 2000.
[36] L. Ljung, System Identification, Theory for the User, second ed., (1999).
[37] C. Pianese, G. Rizzo, Interactive optimization of internal combustion engine tests by means of sequential experiment design, in: Proc. of the 3rd Biennal Joint Conference on 'Engineering Systems Design and Analysis – Esda 96', Petroleum Division of ASME, ASME PD, vol 80, July 1 – 4 1996, pp. 57–64. Montpellier, France.
[38] A. Esposito, P. Moçotéguy, F. Postiglione, M. Guida, C. Pianese, A. Pohjoranta, K. Wang, D. Hissel, M.-C. Péra, S. Pofahl, Experimental test plan and data analysis based on the design of experiment methodology, in: Proceedings of the ASME 2012 6th International Conference on Energy Sustainability & 10th Fuel Cell Science, Engineering and Technology Conference, July 23–26, 2012. San Diego, CA, USA.
[39] I. Arsie, F. Marotta, C. Pianese, G. Rizzo, Journal of Engines 110 (2001) 549–560.
[40] M.L. Gargano, B.G. Raggad, OCLC Systems & Services 15 (1999) 81–90.
[41] S.J. Lee, K. Siau, Industrial Management & Data Systems 101 (2001) 41–46.